

NANOPHOTONICS

Detecting mid-infrared light by molecular frequency upconversion in dual-wavelength nanoantennas

Angelos Xomalis¹, Xuezhi Zheng^{1,2}, Rohit Chikkaraddy¹, Zsuzsanna Koczor-Benda³, Ermanno Miele^{1,4,5}, Edina Rosta³, Guy A. E. Vandenbosch², Alejandro Martínez⁶, Jeremy J. Baumberg^{1*}

Coherent interconversion of signals between optical and mechanical domains is enabled by optomechanical interactions. Extreme light-matter coupling produced by confining light to nanoscale mode volumes can then access single mid-infrared (MIR) photon sensitivity. Here, we used the infrared absorption and Raman activity of molecular vibrations in plasmonic nanocavities to demonstrate frequency upconversion. We converted approximately 10-micrometer-wavelength incoming light to visible light by surface-enhanced Raman scattering (SERS) in doubly resonant antennas that enhanced upconversion by more than 10^{10} . We showed 140% amplification of the SERS anti-Stokes emission when an MIR pump was tuned to a molecular vibrational frequency, obtaining lowest detectable powers of 1 to 10 microwatts per square micrometer at room temperature. These results have potential for low-cost and large-scale infrared detectors and spectroscopic techniques.

Infrared spectroscopy delivers information that is difficult to obtain from other frequency bands, such as atmospheric absorption of molecules (greenhouse gases) or thermally emitted radiation from Earth (meteorological maps or imaging wildfires) (1–5). Although the development of mid-IR (MIR) sources is evolving, a bottleneck continues to be producing low-noise room temperature detectors (6). One proposed scheme is to directly upconvert MIR photons into high-energy visible photons that are efficiently detected, potentially delivering single-photon semiconductor-based detectors (7–9). Analogous wavelength conversion from microwave to optical frequencies has used expensive fabrication and cryogenic temperatures (10, 11), as well as LiNbO₃ resonators (12, 13). To access

the efficiencies required, strongly enhanced light-matter interactions are paramount. Thus, plasmonic devices and planar resonant metasurfaces that confine light have been of interest for MIR-integrated detection and biosensing (14–16).

A promising approach for detecting infrared radiation through frequency upconversion is by molecular optomechanical coupling (17). Optomechanical interactions allow coherent conversion of signals between the optical and mechanical domains (Fig. 1). Nanocavities containing vibrating molecules act as mechanical oscillators, with MIR-absorbing infrared vibrational modes probed by a visible laser through their Raman scattering (Fig. 1B). The required interactions can be boosted by using the tight light localization inside plasmonic nanocav-

ities <100 nm across, which yield detectable signals even from single vibrational bonds (18). The interaction of light and matter in these subnanometer mode volumes gives extreme optomechanical coupling with single MIR-photon sensitivity in principle, but so far this has only been studied theoretically (17). The noise-equivalent power of hybrid nanocavity-molecular detectors is predicted to be 100-fold lower than commercial uncooled detectors.

Of vital importance for upconversion efficiency is the optimal spatial overlap of visible and infrared radiation. Plasmonic nanoparticles allow extreme light confinement at visible frequencies, and at longer wavelengths light localization is challenging but can be achieved with suitable designs (19, 20). Achieving light confinement simultaneously in both visible and MIR spectral regions requires a hybrid dual resonator (21). Here, this was fulfilled by creating doubly resonant antennas that focus long and short wavelengths into the same active region, allowing extreme optomechanical coupling (Fig. 1D). Their construction combines bottom-up and top-down methods that allow for ease of fabrication and cost-effective, large-scale arrays of devices.

To demonstrate MIR detection, we performed surface-enhanced Raman spectroscopy (SERS)

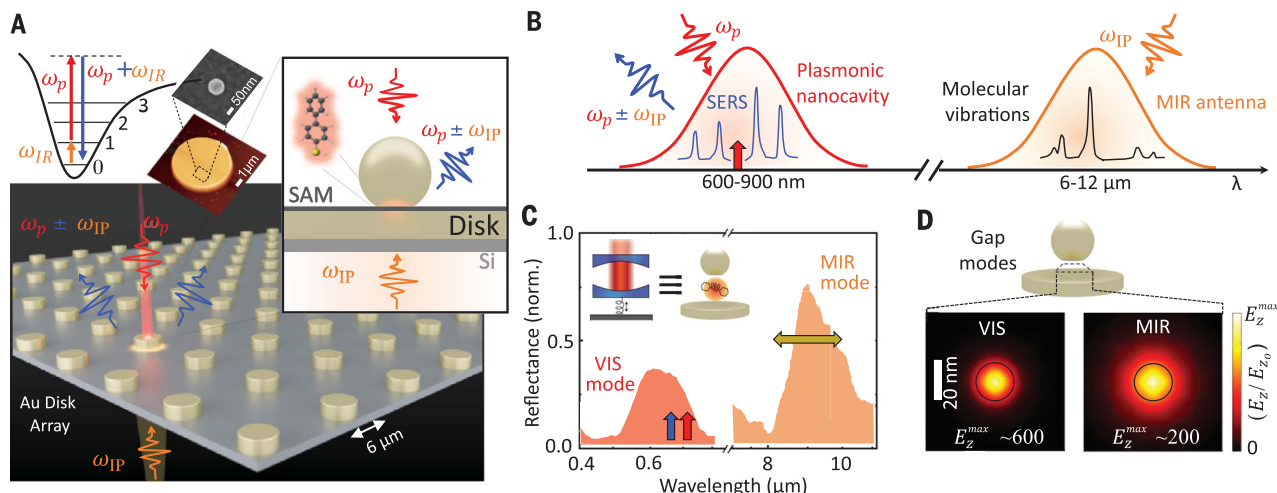


Fig. 1. Dual-wavelength antenna and frequency upconversion. (A) Pump (MIR)–probe (visible) detection configuration. Inset shows upconversion process, AFM (disk) and SEM (nanoparticle) images, and a self-assembled monolayer of BPT creating a 1.3 nm cavity between the 60 nm Au nanoparticle and the 6 μm disk. (B) Scheme of MIR to visible light upconversion through molecular optomechanics. (C) Experimental

reflectance of nanoparticle-on-resonator (NPoR) resonances at both visible (red) and MIR (orange) wavelengths. Arrows indicate SERS probe wavelength (785 nm, red), inelastic scattered light (blue), and MIR tuning range (8.5 to 12.6 μm, yellow). Inset shows equivalence of optomechanical cavity and NPoR. (D) Near-field normalized maps of MIR and visible gap modes of NPoR. Black circle shows a 20 nm nanoparticle facet.

¹NanoPhotonics Centre, Cavendish Laboratory, Department of Physics, University of Cambridge, Cambridge, UK. ²Department of Electrical Engineering (ESAT-TELEMIC), KU Leuven, Leuven, Belgium. ³Department of Physics and Astronomy, University College London, London, UK. ⁴Department of Chemistry, University of Cambridge, Cambridge, UK. ⁵The Faraday Institution, Harwell Science and Innovation Campus, Oxford, UK. ⁶Nanophotonics Technology Center, Universitat Politècnica de València, Valencia, Spain.

*Corresponding author. Email: jjb12@cam.ac.uk

on self-assembled molecular monolayers with discrete vibrational absorption modes in the $\lambda = 6$ to $12 \mu\text{m}$ range. Coupling requires matching the optical (infrared absorption) and mechanical (molecular vibration) energies. Biphenyl-4-thiol (BPT) was chosen (inset, Fig. 1A) because it provides vibrations that are simultaneously active in both IR absorption and Raman and binds strongly and consistently to Au. Integrated into a dual-wavelength Au antenna, called a nanoparticle-on-resonator (NPoR), this strongly confines visible and MIR light within the same active region (21), accessing single-molecule optomechanical nonlinearities (22, 23). The Au disk resonators (diameter $6 \mu\text{m}$) have a fundamental resonant mode around $\lambda = 10 \mu\text{m}$ and high-order modes in the visible spectrum (21). Onto these is self-assembled a molecular monolayer of BPT, with 60 nm Au nanoparticles drop-cast on top. The molecule length sets the 1.3 nm spacing (18), giving resonances that are experimentally measured with visible and MIR light (Fig. 1C). Comparison with simulations shows field enhancements $E/E_0 > 500$ (visible) and >200 (MIR) (fig. S4A) (21), providing a more favorable geometry than previously devised for (simulating) molecular upconversion (17). A modified microscope focuses visible and MIR lasers onto the same NPoR nanodevice (with >40 NPoRs tested here). The 1080 cm^{-1} molecular vibration was observed in SERS anti-Stokes emission, with amplitude that increased linearly when pumped directly with MIR radiation tuned to the same energy.

Our experiments used synchronized visible and quantum cascade laser (QCL) rectangular pulses ($0.4 \mu\text{s}$) to collect SERS spectra with and without the MIR light (Fig. 2). These confirmed the prediction of frequency upconversion (17) using the $\nu = 1080 \text{ cm}^{-1}$ BPT mode, which is both infrared and Raman active (Figs. 3A and 4A). Measuring SERS from NPoRs shows the expected BPT vibrations on both the Stokes and anti-Stokes sides of the laser (Fig. 3B), which are stable and repeatable over long periods. The QCL is then tuned to the same photon energy $h\nu$ (orange, Fig. 3B) and an infrared pump power dependence recorded (Fig. 3C). We found that the anti-Stokes SERS was 100% higher from NPoR₁ when QCL average powers of $5 \mu\text{W}/\mu\text{m}^2$ were incident [Fig. 3D; using peak area ratio $\text{AS}(\text{QCL}_{\text{on}})/\text{AS}(\text{QCL}_{\text{off}})$ with background-subtracted anti-Stokes peaks, peak power is 12 times larger; see materials and methods section S2]. The expected linear dependence of frequency upconversion with pump power was similar for the different NPoRs (red points, Fig. 3C). The lowest detectable light intensity of these dual-wavelength plasmonic antennas was $\sim 1 \mu\text{W}/\mu\text{m}^2$ (Fig. 3C), whereas the lock-in detection synchronized technique here showed that the response speed was submicrosecond,

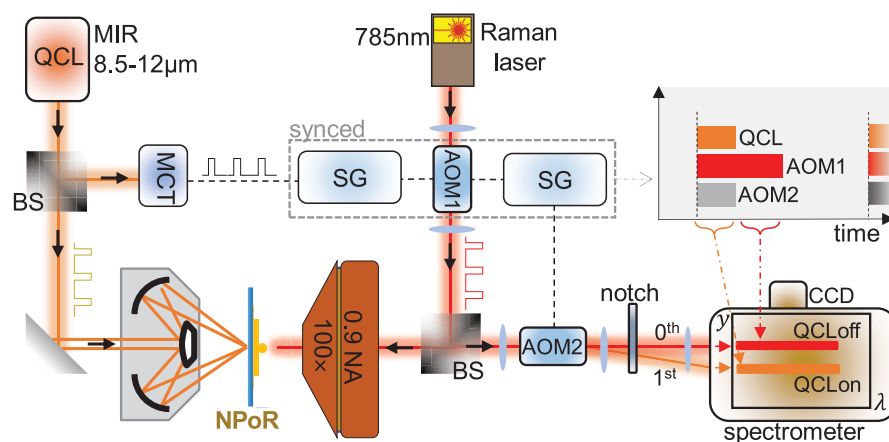


Fig. 2. MIR and visible spectroscopy. Dual microscope combines visible probe and MIR pump for frequency upconversion of molecules in nanogaps: AOM, acousto-optic modulator; MCT, mercury-cadmium-telluride detector; BS, beam splitter; SG, signal generator. Inset: Timing sequence of each repetition of QCL (pump) to Raman laser modulation (AOM1). AOM2 deflects each SERS spectrum to different vertical positions y on the spectrometer slit, extracting Raman spectra versus λ for QCL on/off.

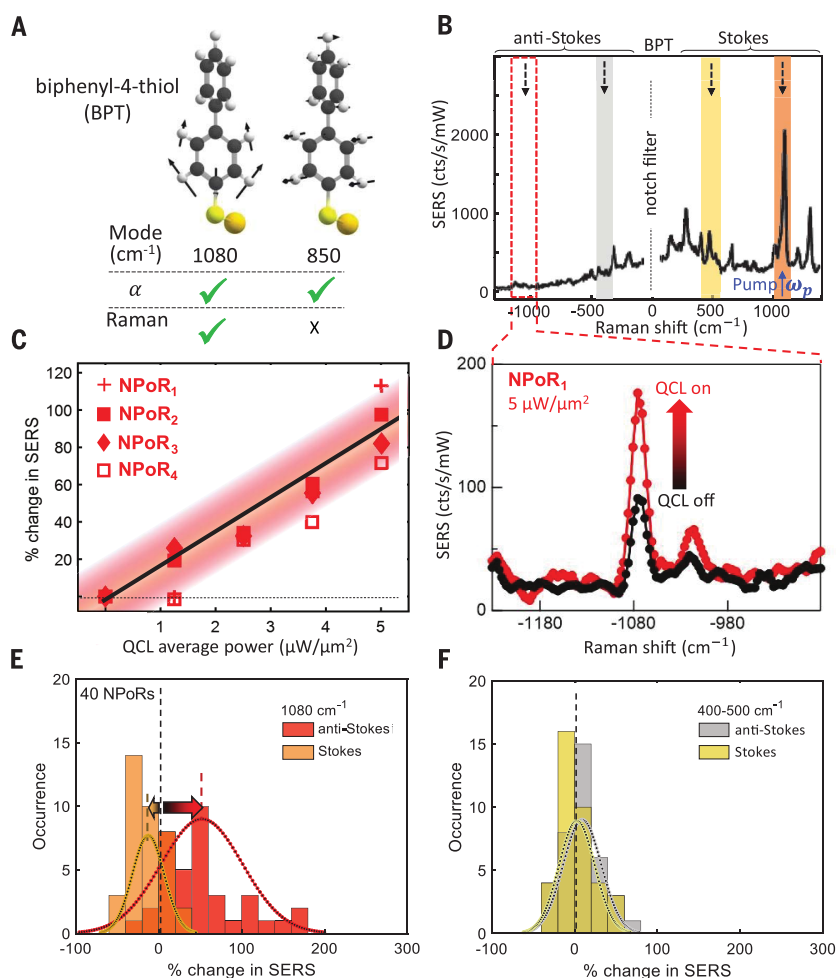


Fig. 3. Upconversion of MIR to visible photons in doubly resonant plasmonic antennas. (A) Vibrations of BPT showing frequencies with strong infrared absorption (α) or Raman. (B) BPT SERS spectrum from the 785 nm probe alone. Shaded regions mark pump (orange, 1080 cm^{-1}) and monitored frequency bands (arrows). (C) Power dependence for four NPoRs. (D) Raw spectra showing the $\nu = 1080 \text{ cm}^{-1}$ anti-Stokes increase when MIR pump is on (red). (E and F) MIR-induced change in SERS of 40 NPoRs at Stokes and anti-Stokes peaks at 1080 cm^{-1} (E) and 400 to 500 cm^{-1} (F).

much faster than the QCL pulse repetition rate (5 μ s).

To better quantify the upconversion efficiency, we measured the percentage change of SERS on 40 NPoRs, where each NP is located at different positions on each disk antenna. These showed an average 52% increase of anti-Stokes at ν (red, Fig. 3E) for 5 μ W/ μ m² MIR average power, whereas the Stokes at ν showed a decrease of 13% (red). No systematic correlation with the nanoparticle position on the disk was apparent, although it likely controls in-coupling of both visible and MIR light into the nanogap.

To confirm the frequency upconversion mechanism, the percentage SERS changes were also extracted for the 400 to 500 cm^{-1} spectral region (yellow and gray shaded areas for Stokes and anti-Stokes, respectively, in Fig. 3B). These low-frequency vibrational modes showed no discernible change within the $\pm 10\%$ signal noise (Fig. 3F). This lack of low wave number signal shows that the signal was not simply thermal heating (fig. S5), as was also suggested by the submicrosecond response, but rather was a nonequilibrium response. If simple heating were involved, then a trebling of anti-Stokes at 1080 cm^{-1} would give a 60% increase at 450 cm^{-1} , which was not observed (see the supplementary materials, section S8).

To understand the frequency-selective dependence, we calculate the product [in $\text{m}^3/(\text{mol}\cdot\text{sr})$] of infrared absorption and Raman intensity of BPT, averaged over all orientations for each normal mode (Fig. 4A and supplementary materials, section S1) (24). This clearly showed that the optimum overlap of optical and vibrational modes was at 1080 cm^{-1} , and that the dipoles were all well aligned with the vertical E field in the nanogap at both visible and MIR wavelengths. To confirm this,

we tuned the QCL from 795 to 1170 cm^{-1} in 15 cm^{-1} steps, ensuring a constant 5 μ W/ μ m² incident on the sample. Although the NPoR device showed a resonant anti-Stokes increase of 140% at 1080 cm^{-1} , it showed no increase elsewhere across the frequency scan (red, Fig. 4B), and neither did the Stokes signal (orange). No clear change in SERS intensity was seen for the 400 to 500 cm^{-1} lines across this MIR tuning on the same NPoR (Fig. 4C). These data clearly distinguish the direct resonant pumping of the optimum 1080 cm^{-1} mode.

The quantum efficiency of these devices was estimated by calibrating to the thermal scale of anti-Stokes emission. At room temperature ($T = 300$ K), with MIR powers of $P = 100$ μ W (intensity $I = 5$ μ W/ μ m²) at 1080 cm^{-1} ($h\nu = 0.13$ eV) and assuming decay times from the first vibrational state of $\tau = 1$ ps (22, 25), using the measured anti-Stokes increase of $\Delta\zeta = 100\%$ (Fig. 3C) gives the fraction of MIR photons arriving that result in an upconverted vibrational response as (see the supplementary materials, section S9)

$$\eta = \Delta\zeta \exp\left\{-\frac{h\nu}{k_B T}\right\} \left[\left(\frac{P}{h\nu}\right)\tau\right]^{-1} \quad (1)$$

corresponding to photon quantum efficiency $\eta \sim 2 \times 10^{-6}$ in this first generation of devices. The induced occupation of the first vibrational level was estimated to be $\Delta\zeta \exp\{-h\nu/k_B T\} \sim 1\%$. Theoretical estimates showed a similar efficiency (17)

$$\eta_t = \eta_{\text{IR}} \eta_0 \frac{g^2 \tau}{\kappa_{\text{IR}}} \sim 1 \times 10^{-6} \quad (2)$$

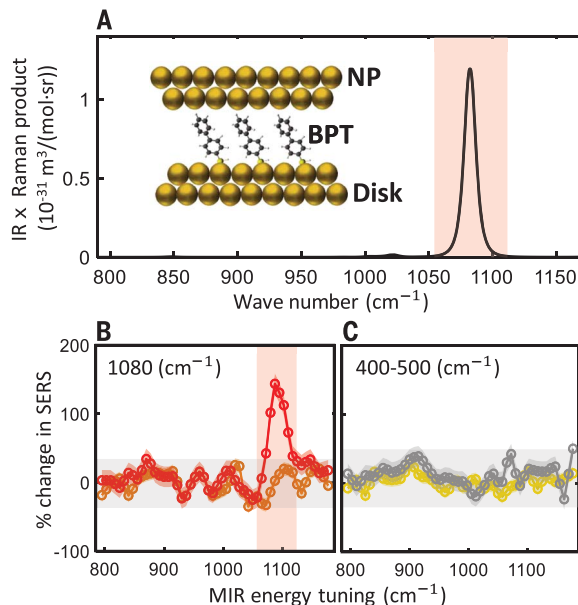
using the measured MIR linewidth (Fig. 1C) to get the antenna loss rate $\kappa_{\text{IR}} \sim 2.7$ THz, an antenna efficiency $\eta_{\text{IR}} \sim 0.5$, and an optomechanical coupling $g \sim 2$ GHz for BPT molecules in the nanocavity gap (22, 23). This assumes that

the optical cross-section of the dual-wavelength antenna matches the incident MIR focus. We estimated the overlap efficiency of nanocavity modes at MIR and Raman wavelengths as $\eta_0 = 66\%$ (see the supplementary materials, section 10), covering ~ 260 BPT molecules. The main inefficiency in η_{IR} was in the fraction of MIR photons giving significant field inside the NPoR gap to vibrationally excite a molecule. Improving the Q factor of the antenna, for example, by using hybridization with photonic cavities, is needed for further enhancements (26). Of 40 measured NPoR devices, 75% showed an upconversion response above the noise (Fig. 3E).

We have also shown that it is possible to fabricate these integrated NPoR detectors using SiN waveguides on standard 4-inch Si wafers (27) in a cheap and scalable combination of top-down and bottom-up lithographies (fig. S3). Prospects for multiband operation are promising [selection of optimal molecules is required to broaden the vibrational range and responsivity (24)] because lower-frequency anti-Stokes emission has already been observed at 250 cm^{-1} (Fig. 3B, $\lambda = 40$ μ m or 7.5 THz). Using alternative molecules embedded in NPoRs, SERS lines observed at ~ 160 cm^{-1} can access targets for astronomical detectors (OH line at 4.7 THz and lower). Although the lifetime of such devices is not yet fully characterized, it already exceeds 1 month, extended by suitable encapsulation to exclude oxygen. The rapid relaxation of nonresonant molecules in the virtual Raman process is encouraging for engineering robust performance. We emphasize that further increases in sensitivity can come from exploiting single-atom picocavities, which deliver 100-fold larger SERS signals from the enhanced light localization around single Au adatoms (28, 29), with simple estimates based on Eq. 2 using the measured $g \sim 5$ THz (22, 23) giving near unity upconversion efficiencies. This makes current efforts to stabilize picocavities significant and optimizes the overlap of MIR light in the same volume.

Fig. 4. MIR tuning dependence of upconversion in NPoR plasmonic construct.

(A) Calculated product of molecular infrared absorption and Raman cross-section for BPT in plasmonic nanogaps (inset). (B and C) Percentage change in SERS from illuminated NPoR versus MIR frequency of 1080 cm^{-1} Stokes (orange) and anti-Stokes (red) peaks (B), as well as 400 to 500 cm^{-1} Stokes (yellow) and anti-Stokes (gray) peaks (C).



REFERENCES AND NOTES

- M. J. Elrod, *J. Chem. Educ.* **76**, 1702 (1999).
- A. Kuze, H. Suto, M. Nakajima, T. Hamazaki, *Appl. Opt.* **48**, 6716–6733 (2009).
- R. S. Allison, J. M. Johnston, G. Craig, S. Jennings, *Sensors* **16**, 1310 (2016).
- W. R. Bandeen, R. Hanel, J. Licht, R. Stampfl, W. Stroud, *J. Geophys. Res.* **66**, 3169–3185 (1961).
- R. Hanel et al., *J. Geophys. Res.* **77**, 2629–2641 (1972).
- A. Rogalski, *Infrared Phys. Technol.* **43**, 187–210 (2002).
- J. S. Dam, P. Tidemand-Lichtenberg, C. Pedersen, *Nat. Photonics* **6**, 788–793 (2012).
- I. Kviatkovsky, H. M. Chrzanoski, E. G. Avery, H. Bartolomaeus, S. Ramelow, *Sci. Adv.* **6**, eabd0264 (2020).
- S. Junaid et al., *Optica* **6**, 702–708 (2019).
- M. Forsch et al., *Nat. Phys.* **16**, 69–74 (2020).
- J. Bochmann, A. Vainsencher, D. D. Awschalom, A. N. Cleland, *Nat. Phys.* **9**, 712–716 (2013).
- W. Jiang et al., *Nat. Commun.* **11**, 1166 (2020).
- L. Shao et al., *Optica* **6**, 1498–1505 (2019).
- F. Yesilkoy et al., *Nat. Photonics* **13**, 390–396 (2019).
- A. Titti et al., *Science* **360**, 1105–1109 (2018).

16. B. Schwarz *et al.*, *Nat. Commun.* **5**, 4085 (2014).
17. P. Roelli, D. Martin-Cano, T. J. Kippenberg, C. Galland, *Phys. Rev. X* **10**, 031057 (2020).
18. J. J. Baumberg, J. Aizpurua, M. H. Mikkelsen, D. R. Smith, *Nat. Mater.* **18**, 668–678 (2019).
19. O. D. Miller *et al.*, *Opt. Express* **24**, 3329–3364 (2016).
20. R. Chikkaraddy, A. Xomalis, L. A. Jakob, J. J. Baumberg, Mid-infrared-perturbed molecular vibrational signatures in plasmonic nanocavities. arXiv:2108.10171 [physics.optics] (2021).
21. A. Xomalis *et al.*, *Nano Lett.* **21**, 2512–2518 (2021).
22. A. Lombardi *et al.*, *Phys. Rev. X* **8**, 011016 (2018).
23. F. Benz *et al.*, *Science* **354**, 726–729 (2016).
24. Z. Koczor-Benda *et al.*, *Phys. Rev. X* (2021).
25. S. Yampolsky *et al.*, *Nat. Photonics* **8**, 650–656 (2014).
26. A. I. Barreda, M. Zapata-Herrera, I. Palstra, L. Mercadé, J. Aizpurua, A. F. Koenderink, A. Martínez, Hybrid photonic-plasmonic cavities based on the nanoparticle-on-a-mirror configuration. arXiv:2106.01931 [physics.optics] (2021).
27. J. Losada *et al.*, *IEEE J. Sel. Top. Quantum Electron.* **25**, 1–6 (2019).
28. T. Wu, W. Yan, P. Lalanne, *ACS Photonics* **8**, 307–314 (2021).
29. T. Wu, M. Gurioli, P. Lalanne, *ACS Photonics* **8**, 1522–1538 (2021).
30. Data for: A. Xomalis, X. Zheng, R. Chikkaraddy, Z. Koczor-Benda, E. Miele, E. Rosta, G. A. E. Vandenbosch, A. Martínez, J. J. Baumberg, Detecting mid-infrared light by molecular frequency upconversion in dual-wavelength nanoantennas, University of Cambridge Repository (2021); <https://doi.org/10.17863/CAM.77640>.

ACKNOWLEDGMENTS

Funding: This work was supported by the European Union's Horizon 2020 Research and Innovation Program under grant agreements 829067 (THOR), 861950 (POSEIDON), and 883703 (PICOFORCE) and by the Engineering and Physical Sciences Research Council (EPSRC) (Cambridge NanoDTC grants EP/L015978/1, EP/L027151/1, EP/S022953/1, EP/P029426/1, and EP/R020965/1). X.Z. acknowledges support from KU Leuven Internal Funds C14/19/083, IDN/20/014, KA/20/019, and FWO G090017N. R.C. acknowledges support from Trinity College, University of Cambridge. Z.K.B. and E.R. acknowledge funding from the EPSRC (EP/R013012/1, EP/L027151/1) and ERC project 757850 BioNet. We are grateful to the UK Materials and Molecular Modelling Hub, which is partially funded by EPSRC (EP/P020194/1),

for computational resources. **Author contributions:** A.X. fabricated the devices, performed the experiments, and analyzed the data. Z.X. and G.V. did electromagnetic calculations. R.C. and A.X. did full-wave simulations. S.K.B. performed DFT calculations. E.M. and A.X. performed SERS of NPoR on Si chips. E.R., A.M., and J.J.B. designed and supervised the work. All authors discussed the results, provided feedback, and contributed to the writing of the manuscript. **Competing interests:** The authors declare no competing interests. **Data and materials availability:** All data needed to evaluate the conclusions in the study are present in the main text or the supplementary materials. Source data can be found at the University of Cambridge Repository (30).

SUPPLEMENTARY MATERIALS

science.org/doi/10.1126/science.abk2593

Materials and Methods

Supplementary Text

Figs. S1 to S10

References (31–42)

6 July 2021; accepted 12 October 2021

10.1126/science.abk2593

Detecting mid-infrared light by molecular frequency upconversion in dual-wavelength nanoantennas

Angelos Xomalis Xuezheng Zheng Rohit Chikkaraddy Zsuzsanna Koczor-Benda Ermanno Miele Edina Rosta Guy A. E. Vandenbosch Alejandro Martínez Jeremy J. Baumberg

Science, 374 (6572), • DOI: 10.1126/science.abk2593

Optomechanical upconversion

Molecules have rich signatures in their spectra at infrared wavelengths and are typically accessed with dedicated spectroscopic instrumentation. Chen *et al.* and Xomalis *et al.* report optomechanical frequency upconversion from the mid-infrared to the visible domain using molecular vibrations coupled to a plasmonic nanocavity at ambient conditions (see the Perspective by Gordon). Using different nanoantenna designs, one with a nanoparticle-on-resonator and the other with nanoparticle-in-groove, both approaches show the ability to upconvert the mid-infrared vibrations of the molecules in the nanocavity to visible light wavelengths. The effect could be used to simplify infrared spectroscopy, possibly with single-molecule sensitivity. —ISO

View the article online

<https://www.science.org/doi/10.1126/science.abk2593>

Permissions

<https://www.science.org/help/reprints-and-permissions>

Use of this article is subject to the [Terms of service](#)

Science (ISSN) is published by the American Association for the Advancement of Science, 1200 New York Avenue NW, Washington, DC 20005. The title *Science* is a registered trademark of AAAS.

Copyright © 2021 The Authors, some rights reserved; exclusive licensee American Association for the Advancement of Science. No claim to original U.S. Government Works